

# A Planar Windmill-Like Broadband Antenna Equipped With Artificial Magnetic Conductor for Off-Body Communications

XiongYing Liu, *Member, IEEE*, YunHui Di, Hui Liu, ZeTao Wu, and Manos M. Tentzeris, *Fellow, IEEE*

**Abstract**—A broadband antenna inspired by a windmill sail is developed for wireless body area network (WBAN) applications. The antenna consists of a couple of modified dipoles with four crossed symmetrical S-shaped arms printed on a flexible substrate. A  $5 \times 5$  unit structure of artificial magnetic conductor (AMC) is integrated to reduce the backward scattering wave toward the human body, and simultaneously ensures a low profile with a thickness of 5.74 mm and a small size with the area of  $46 \times 46 \text{ mm}^2$ . The measured results on the phantom reveal that the AMC-integrated antenna accomplishes an impedance bandwidth of 63.5% (5.7–11.0 GHz) with  $S_{11} < -10 \text{ dB}$ , a peak gain of 8 dBi, and a front-to-back ratio (FBR) greater than 15 dB. Health safety factors, such as specific absorption rate and temperature, are considered. According to the calculation of link budget in different scenarios, the reliable communication can be guaranteed within 10 m in line-of-sight (LOS) environment. The good performances make the proposed AMC-integrated antenna potential for wireless communication between miniaturized wearable sensors and a localized base station around body.

**Index Terms**—Artificial magnetic conductor (AMC), broadband antenna, link budget, temperature, wireless body area network (WBAN).

## I. INTRODUCTION

FOR the fixture on the body, wearable antennas in wireless body area network systems (WBANs) are faced with the challenges of light weight, flexibility, low profile, and reliable communications [1]. Severe conditions, such as requirement of low health hazard and influence caused by the lossy tissues, complicate the design of radio transceiver. The antenna in ultrawideband (UWB) is an upcoming wireless technology appropriate for WBAN, due to its compact, low emission power, and large channel capacity. Several UWB antennas for WBAN have been proposed. In [2], a coplanar waveguide (CPW)-fed textile antenna can operate in the entire UWB band. Meanwhile, backward radiation is identical to forward radiation. To decrease

Manuscript received February 10, 2015; revised March 25, 2015; accepted May 02, 2015. Date of publication May 05, 2015; date of current version February 04, 2016. This work was supported in part by the National Natural Science Foundation of China under Grant 61372008, the Fundamental Research Funds for the Central Universities under Grant 2014ZZ0031, and the National Engineering Technology Research Center for Mobile Ultrasonic Detection.

X. Liu, Y. Di, H. Liu, and Z. Wu are with the School of Electronic and Information Engineering, South China University of Technology, Guangzhou 510640, China, and also with the State Key Laboratory of Millimeter Waves, Nanjing 210096, China (e-mail: liuxy@scut.edu.cn).

M. M. Tentzeris is with the School of Electrical and Computer Engineering, Georgia Institute of Technology, Atlanta, GA 30332 USA.

Color versions of one or more of the figures in this letter are available online at <http://ieeexplore.ieee.org>.

Digital Object Identifier 10.1109/LAWP.2015.2429683

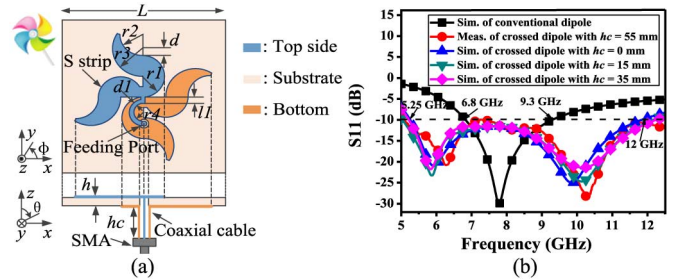


Fig. 1. (a) Geometry of the proposed dipole antenna and picture of windmill. (b)  $S$ -parameters of the crossed dipole with different  $h_c$  and traditional dipole.

the coupling with the body, a vertically-polarized 8.5-mm-high antenna with at least  $64 \times 64 \text{ mm}^2$  ground plane is presented in [3]. In [4], a 3-D directional antenna with a peak gain of 5.8 dBi is investigated. We have designed a triple-band antenna. Due to the mismatch and loss caused by the proximity to human body, it has a low gain of about  $-2 \text{ dBi}$  and has to keep a certain distance away from the skin [5].

Artificial magnetic conductor (AMC) with the characteristic of in-phase reflection can maintain appropriate shielding for the biological tissues beneath the antennas and guide the electromagnetic wave into the upper-half space [6]. Wearable antennas based on AMC with narrowband characteristics have been proposed. In [7], a dual-band (i.e., 2.45 and 5 GHz) textile antenna with a dimension of  $120 \times 120 \text{ mm}^2$ , based on the electromagnetic band-gap (EBG), is investigated. In [8], a single-band monopole antenna with an 18% impedance bandwidth, located above an AMC ground plane with *Jerusalem Cross* geometry, is studied.

To keep the advantages and overcome the defects in the aforementioned literature, a windmill-shaped dipole with an AMC reflector is investigated. The AMC-integrated antenna has a compact dimension, low profile, high gain, and slight electromagnetic radiation on the body. In Section II, the design and analysis of the proposed antenna and AMC are investigated. Measured results, such as  $S_{11}$ , bending characteristic, safety consideration, radiation pattern, and link budget, are analyzed in Section III. Finally, conclusions are given in Section IV.

## II. DESIGN AND CONFIGURATION

### A. Antenna Design

As exhibited in Fig. 1(a), the structure of the crossed symmetrical dipole antenna is composed of four S-shaped strips, which are etched on both sides of a flexible Panasonic R-F770 substrate with  $\epsilon_r = 3.2$ ,  $\tan \delta = 0.002$ . Each S-shaped arm of the

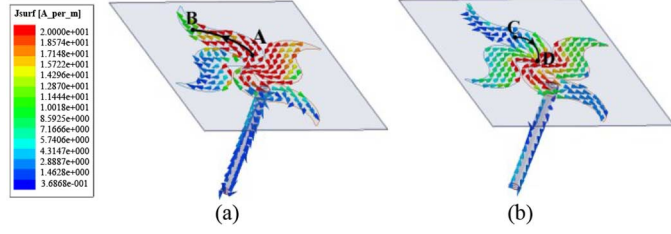


Fig. 2. Current distribution on the antenna arms and the outer conductor of the feeding coaxial cable at (a) 6 and (b) 10 GHz.

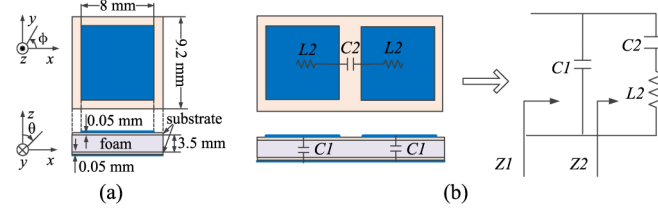


Fig. 3. (a) Configuration and (b) equivalent circuit of adjacent square-shaped AMC units.

dipoles mainly contributes to diminish the size and smoothing current path. An annular microstrip line is terminated with two interconnecting S-shaped strips on the top side of the substrate. At the feeding port, a hole on the substrate is drilled, through which the inner conductor of a flexible 50- $\Omega$  coaxial cable is connected to the annular microstrip line on the front side, while the outer conductor is soldered to the S-shaped strips on the back side. The whole configuration looks like a windmill sail and has an aesthetic sense.

With reference to Fig. 2, it can be seen that the S-shaped strips in the up-down direction have parallel current as the strips on the right and left, hence strengthening the radiation. Simultaneously, short current path (e.g., arc CD) corresponds to upper resonant frequency, and long current path (e.g., arc AB) is for the lower. For the electromagnetic (EM) coupling between crossed dipoles, resonant frequencies are close to each other, hence broadening the band. The proposed dipole has a bandwidth of 78.3% (5.25–12 GHz), more than double that (31%, or 6.8–9.3 GHz) of single conventional dipole, and the measured  $S_{11}$  agrees well with the simulated one in free space. As illustrated in Fig. 2, the current on the outer conductor of coaxial cable is very weak, compared to that on dipole arms. To further study the effect of the coaxial cable, the  $S$ -parameters with varied lengths of  $hc$  are analyzed in Fig. 1(b). It can be seen that although the curves fluctuate as  $hc$  varies,  $S_{11}$  is still less than  $-10$  dB in the required band. In principle, this is due to the fact that the feeding port of the proposed dipole antenna is not located in the center of two arms, making the signal on arms unbalanced. Hence, a balun is redundant to avoid the radiation caused by the outer conductor of coaxial cable. After the tradeoff between easiness of fabrication and enhancement of performance has been made, the following optimized values with the aid of ANSYS HFSS ver. 13 are obtained:  $L = 26$  mm,  $r1 = 3.6$  mm,  $r2 = 3.5$  mm,  $r3 = 5.2$  mm,  $r4 = 2.05$  mm,  $d = 1$  mm,  $d1 = 0.35$  mm,  $l1 = 0.7$  mm, and  $h = 0.14$  mm.

### B. AMC Design

The geometry of the AMC element is shown in Fig. 3(a). It is composed of three layers without metal-via connection. The top layer is a square-shaped patch sculptured on a flexible Panasonic R-F770 substrate. The bottom is a grounded Panasonic R-F770

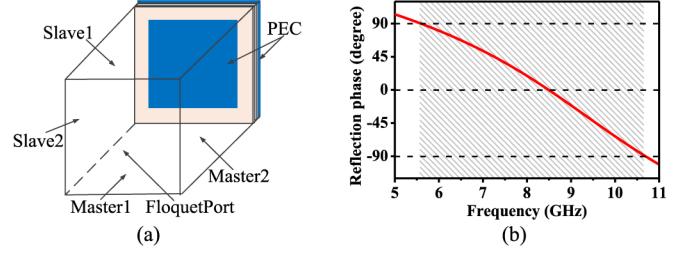


Fig. 4. (a) Model used for the simulation. (b) Reflection phase over the frequency band.

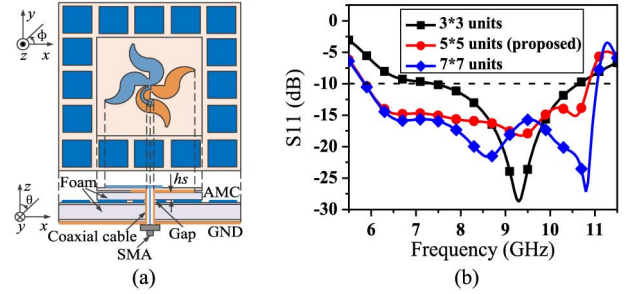


Fig. 5. (a) Configuration of the AMC-integrated antenna. (b)  $S$ -parameters of the proposed antenna with different AMC ground plane size.

substrate with the same thickness as the top. For the characteristics of light weight, flexibility, adequate toughness, and electric properties similar to air, a piece of flexible ethylene-vinyl acetate (EVA) foam with  $\epsilon_r = 1.17$ ,  $\tan \delta = 0.002$  is filled in the interlayer. Though analyzing the working principle in [9], the EM field in AMC structure can be simplified to the circuit model given in Fig. 3(b). Thus, its total surface impedance can be expressed as

$$Z_0(\omega) = Z_1 // Z_2 = \frac{j(1 - \omega^2 C_1 L_2)}{\omega(C_1 C_2 L_2 \omega^2 - C_1 - C_2)}. \quad (1)$$

From (1), the resonant frequency of the construction can be calculated as

$$f_0 = \frac{1}{2\pi} \sqrt{\frac{C_1 + C_2}{C_1 C_2 L_2}} \quad (2)$$

where  $C_1$ ,  $L_2$ ,  $C_2$  are the capacitance between patch and ground plane, unit inductance, and capacitance between units, respectively.

As depicted in Fig. 4(a), the model based on a floquet-port air-filled waveguide with master-slave boundary conditions is adopted for numerically computing the reflection phase of AMC. With reference to Fig. 4(b), the band 5.6–10.6 GHz with the reflection phases of between  $\pm 90^\circ$  is covered.

### C. Integration of Antenna and AMC

To alleviate the EM wave transmission into body and further strengthen the forward radiation, an AMC array acting as an in-phase reflector for the proposed antenna is designed. As shown in Fig. 5(a), the crossed dipole is suspended at a distance of  $hs = 2$  mm (less than a quarter-wavelength at 11 GHz) from the top of the AMC surface. Here, a block of flexible EVA foam is utilized to hold and isolate the antenna from the AMC, simultaneously reducing the impedance mismatch caused by the proximity of AMC. In addition to being a low profile, the proposed antenna should be small area. Therefore, the performance of  $S_{11}$  under different AMC sizes is analyzed. As plotted in Fig. 5(b), an array of  $5 \times 5$  units is acceptable.



Fig. 6. Photographs of experiments using (a) Agilent N5 230A vector network analyzer and (b) SPEAG DASY5 SAR measurement system.

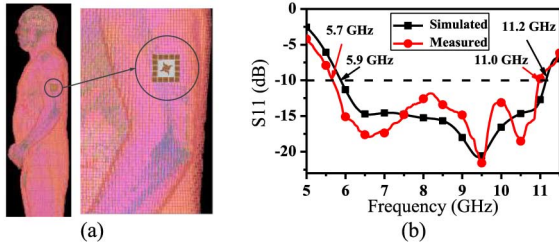


Fig. 7. (a) Numerical inhomogeneous human model used for validating the capability of the proposed antenna in XFDTD. (b) Performance of  $S_{11}$ .

### III. EXPERIMENTAL RESULTS AND ANALYSIS

After the theoretical design, the prototype of proposed antenna has been fabricated. Impedance matching and EM radiation were measured using experimental equipment shown in Fig. 6(a) and (b), respectively.

#### A. S-Parameters on the Body

To accurately analyze the effects of an inhomogeneous body on the performance, the model of AMC-integrated antenna was imported to XFDTD [10] and simulated over a numerical 3-D volume with an approximate data set of the human tissues. As shown in Fig. 7(a), the antenna is positioned on the upper arm. To reduce the calculating time, the concerned part of the body is selected instead of the whole numerical phantom. With reference to the Fig. 7(b), the simulated bandwidth of 61.9% (5.9–11.2 GHz) with  $S_{11} < -10$  dB, close to the measured bandwidth of 63.4% (5.7–11.0 GHz), which is wide enough for off-body communications, simultaneously complying with EM spectrum regulation in Europe and USA, etc. The divergence is mainly attributed to the fabrication tolerance.

#### B. Conformability to the Body

For convenience and comfort, the wearable antenna has to be conformal to the body. To validate its stability in diverse conditions, bending effect on the antenna performance is studied. A cylindrical three-layer human tissue model with a radius of  $R$  is employed to mimic the body. Three situations with different curvatures shown in Fig. 8(a), representing the detailed setup positions on body, are simulated. As depicted in Fig. 8(b), the performance is insensitive to the antenna's deforming. Since the dielectric properties of human tissues are dependent of EM frequency, a parametric model for the complex relative permittivity as a function of angular frequency has been developed by Gabriel *et al.* with a Cole-Cole equation [11]. Hence, during the simulation, the specific  $S_{11}$  at certain frequency is computed with different electric parameters.

#### C. Safety Consideration

Since the EIRP spectral density of the proposed antenna is no more than  $-41.3$  dBm/MHz regulated by the FCC, SAR may

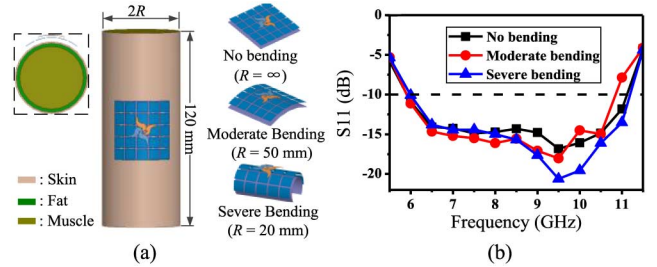


Fig. 8. (a) Phantom and different bending conditions simulated in HFSS. (b) Simulated  $S_{11}$  with different bending conditions on human tissue with frequency-dependent electric parameters.

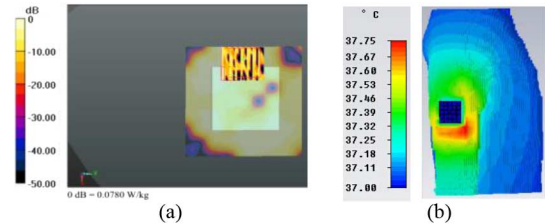


Fig. 9. (a) Measured SAR for the AMC-integrated antenna at 6 GHz. (b) Temperature variation with an input power that causes a maximum SAR of 1.6 W/kg at 6 GHz.

not exceed 1.6 W/kg, as verified in Fig. 9(a). However, the absorbed radiation power of the proposed antenna by tissues will translate into heat loss. A subsequent temperature increase of more than  $1^{\circ}\text{C}$ – $2^{\circ}\text{C}$  in the tissues will cause adverse health effects [12]. A severe case under the condition of an input RMS power of 1.56 W that may cause a maximum SAR of 1.6 W/kg with 1 g averaging mass is investigated, using thermal transient solver in CST, which has taken into account heat loss in the body and the bio-heat effects caused by cell metabolism and blood flow. As depicted in Fig. 9(b), when initial temperature of  $37^{\circ}\text{C}$  is set, the maximum temperature rise over the period of 6 min is less than  $0.75^{\circ}\text{C}$ . Also, due to the antenna's exposure to the air and clothes' isolation, the temperature cannot be aggregated as time goes on.

#### D. Properties of Far-Field Radiation

Due to the proposed antenna's operation in wireless frequencies with centimeter wavelength, we adopted an elevated outdoor far-field setup with virtually eliminated ground and stray wave effects in the radiation pattern measurement. Compared to the antenna without AMC, the radiation patterns of the AMC-integrated antenna are almost unidirectional with the front-to-back ratio (FBR) more than 15 dB, as shown in Fig. 10. Small differences between the measured and simulated radiation patterns may be attributed to the measurement environment and lossy human body. The measured radiation properties of the proposed antenna with and without AMC on the body are compared in Table I. Since the body absorbs more EM wave of antenna without AMC than with AMC, the peak gains and FBRs of antenna with AMC on the body are larger than those of antenna without AMC.

#### E. Link Budget of the AMC-Integrated Antenna

Through taking logarithm, the Friis transmission formula under the condition of good impedance matching is [13]

$$P_r [\text{dBm}] = P_t [\text{dBm}] + G_t [\text{dB}] - PL_{\text{dB}}(d) + G_r [\text{dB}] \quad (4)$$

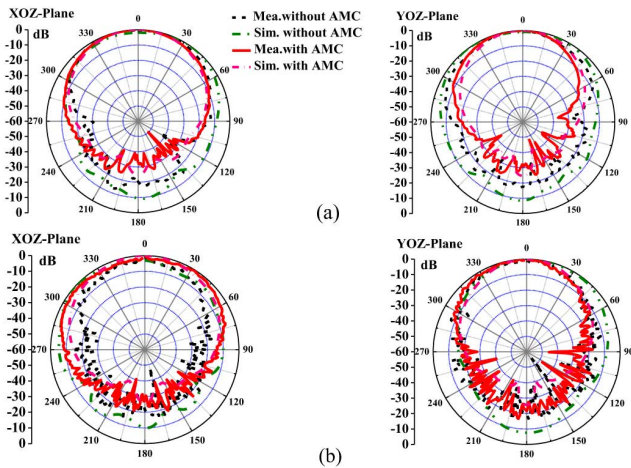


Fig. 10. Measured and simulated radiation patterns of the proposed antenna with or without AMC on the body at (a) 7 and (b) 10 GHz.

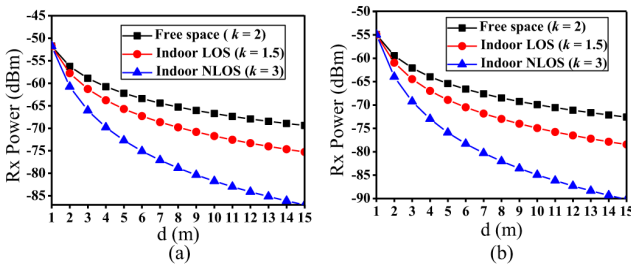


Fig. 11. Calculated received power ( $P_r$ ) for three scenarios at (a) 7 and (b) 10 GHz.

TABLE I

RADIATION PERFORMANCES OF THE ANTENNA IN DIFFERENT CONDITIONS

Frequency (GHz)	Antenna without AMC			AMC-integrated antenna		
	Peak Gain (dBi)	Efficiency (%)	FBR (dB)	Peak Gain (dBi)	Efficiency (%)	FBR (dB)
7	2.8	31.2 %	16.9	8.0	90.6 %	24.8
8.5	3.5	39.1 %	11.9	7.5	83.8 %	16.4
10	6.8	75.9 %	14.7	7.6	85.5 %	18.5

and considering the multipath propagation environment

$$PL_{dB}(d) = 10k \log\left(\frac{d}{d_0}\right) + 10 \log\left(\frac{4\pi d_0}{\lambda}\right)^2 + \chi_\sigma \quad (5)$$

where  $P_t$  and  $P_r$  represent the transmitted (Tx) and received (Rx) power, respectively;  $G_t$  and  $G_r$  are the corresponding Tx and Rx antenna gains;  $\lambda$  is the wavelength in free space, and  $d$  is the distance between Tx and Rx antennas. Here,  $d_0 = 1$  m is used as the reference distance,  $\chi_\sigma$  is the shadowing factor of Gaussian distribution with a standard deviation  $\sigma$ , and  $k$  represents path-loss decay depending on the different propagation scenarios, such as in free space ( $k = 2$ ), indoor line-of-sight (LOS) path ( $k = 1.5$ ), e.g., stadium, and indoor non-line-of-sight (NLOS) condition ( $k = 3$ ), e.g., meeting room.

When the AMC-integrated antenna acts as a transmitting terminal, the received power ( $P_r$ ) can be calculated with  $P_t = -12.06$  dBm and  $G_r = 2.15$  dBi using the expressions (4) and (5). Due to reflection, diffraction, and scattering of electromagnetic waves in indoor environments, the transmitted signal reaches receiver via multipath. Thus, the received power  $P_r$  in indoor environments degrades faster than that in free space, which can be seen in Fig. 11. The received power  $P_r$  of the LOS

link is higher than that of NLOS link at 7 and 10 GHz since the obstacles in NLOS environment make EM waves decay more. Especially in a densely furnished room, with more obstacles between the transmitter and receiver, the surrounding environment can produce a destructive effect to the received power. Assuming the minimum receiver sensitivity is  $-75$  dBm, the distance for reliable communication can be realized within 10 m in indoor LOS environment.

#### IV. CONCLUSION

This letter has studied a flexible crossed-dipole antenna with a shape of windmill. It has advantages of compact and broadband over traditional dipole. Simultaneously, the artistic look can avoid visual pollution. To realize off-body communications, a square-shaped AMC plane, instead of PEC ground, is equipped. Due to the characteristics of in-phase reflection, the introduced AMC reflector not only protects human body, but also keeps the proposed antenna close to skin, hence obtaining a low profile. The conformability to body and the stability in varied situations reveal that the AMC-integrated antenna is robust to deformation. The performance of SAR and temperature illustrates EM-radiation safety. Through the analysis of link budget, the wireless communication between the AMC-integrated antenna and nearby radio transceiver within a large scope in indoor LOS environment is realizable. Therefore, the AMC-integrated antenna can be a good candidate for off-body communications in WBAN systems.

#### REFERENCES

- [1] P. S. Hall and Y. Hao, *Antennas and Propagation for Body-Centric Wireless Communications*, 2nd ed. Norwood, MA, USA: Artech House, 2012.
- [2] M. Klemm and G. Troester, "Textile UWB antennas for wireless body area networks," *IEEE Trans. Antennas Propag.*, vol. 54, no. 11, pp. 3192–3197, Nov. 2006.
- [3] M. Koohestani, J. F. Zürcher, A. A. Moreira, and A. K. Skrivervik, "A novel, low-profile, vertically-polarized UWB antenna for WBAN," *IEEE Trans. Antennas Propag.*, vol. 62, no. 4, pp. 1888–1894, Apr. 2014.
- [4] C. H. Kang, S. J. Wu, and J. H. Tarnag, "A novel folded UWB antenna for wireless body area network," *IEEE Trans. Antennas Propag.*, vol. 60, no. 2, pp. 1139–1142, Feb. 2012.
- [5] C. P. Deng, X. Y. Liu, Z. K. Zhang, and M. M. Tentzeris, "A miniscape-like triple-band monopole antenna for WBAN applications," *IEEE Antennas Wireless Propag. Lett.*, vol. 11, pp. 1330–1333, 2012.
- [6] A. Foroozesh and L. Shafai, "Investigation into the application of artificial magnetic conductors to bandwidth broadening, gain enhancement and beam shaping of low profile and conventional monopole antennas," *IEEE Trans. Antennas Propag.*, vol. 59, no. 1, pp. 4–20, Jan. 2011.
- [7] S. Zhu and R. Langley, "Dual-band wearable textile antenna on an EBG substrate," *IEEE Trans. Antennas Propag.*, vol. 57, no. 4, pp. 926–935, Apr. 2009.
- [8] H. R. Raad, A. I. Abbosh, H. M. Al-Rizzo, and D. G. Rucker, "Flexible and compact AMC based antenna for telemedicine applications," *IEEE Trans. Antennas Propag.*, vol. 61, no. 2, pp. 524–531, Feb. 2013.
- [9] Y. Zhang, J. von Hagen, M. Younis, C. Fischer, and W. Wiesbeck, "Planar artificial magnetic conductors and patch antennas," *IEEE Trans. Antennas Propag.*, vol. 51, no. 10, pp. 2704–2712, Oct. 2003.
- [10] XFDTD EM Simulation Software Remcom, State College, PA, USA [Online]. Available: <http://www.remcom.com/xft7>
- [11] S. Gabriel, R. W. Lau, and C. Gabriel, "The dielectric properties of biological tissues: III. Parametric models for the dielectric spectrum of tissues," *Phys. Med. Biol.*, vol. 41, no. 11, pp. 2271–2293, 1996.
- [12] K. M. S. Thothahewa, J.-M. Redouté, and M. R. Yuce, "SAR, SA, and temperature variation in the human head caused by IR-UWB implants operating at 4 GHz," *IEEE Trans. Microw. Theory Tech.*, vol. 61, no. 5, pp. 2161–2169, May 2013.
- [13] A. Sani, A. Alomainy, and Y. Hao, "Numerical characterization and link budget evaluation of wireless implants considering different digital human phantoms," *IEEE Trans. Microw. Theory Tech.*, vol. 57, no. 10, pp. 2605–2613, Oct. 2009.